Semianalytic theory of Rydberg electron diamagnetism

U. Fano and E. Y. Sidky
Department of Physics and The James Franck Institute, The University of Chicago, 5640 South Ellis Avenue, Chicago, Illinois 60637
(Received 26 August 1991)

The dynamics of a Rydberg electron in a magnetic field is examined for clues to the analytic structure of the electron wave function. A multichannel phase-amplitude formulation proves successful in the intermediate range of radial distances, where the onset of diamagnetism reshapes the Coulomb wave functions. Numerical integration of first-order equations in this range serves to illustrate the evolution of wave functions.

PACS number(s): 31.15.+q, 32.60.+i, 34.10.+x

I. INTRODUCTION

The diamagnetism of a Rydberg electron involves a boost of its kinetic energy stemming from Larmor precession; this boost is proportional to the squared flux of a magnetic field **B** threaded through the electron's orbital. The onset of a magnetic field also warps the otherwise spherical symmetry of this orbital, a symmetry familiarly described by a spherical harmonic $Y_{lm}(\theta,\varphi)$. For an electron excited by a photon with linear polarization parallel to **B**, i.e., along $\theta=0$, the warping replaces—at sufficiently large r—the spherical distribution $Y_{lm}(\theta,\varphi)$ by a cylindrical oscillator's Hermite-like function $G_{lm}(Br\sin\theta,\varphi)$, which represents a Landau orbital. This replacement is accompanied by a modest distortion of the relevant Coulomb radial function $F(r)$ into an analogous $F(r\cos\theta)$. [Note that Landau oscillation amplitudes are $O(100$ a.u.) for strong laboratory fields.] The corresponding warp for a polarization orthogonal to **B** is more novel and radical, replacing Y_{lm} by an orbital analogous to $G_{lm}(Br\cos\theta,\varphi)$, and forcing $F(r)$ to turn progressively, at large r, from a Coulomb into an oscillator function of $r\sin\theta$. The latter orbitals have been dubbed "quasi-Landau."

The widespread occurrence of orbital warping, as an excited particle (or aggregate) becomes exposed to fields of different symmetry, has been stressed by Rau [1]. The novel aspects of high Rydberg diamagnetism were initially detected and interpreted by Jenkins and Segrè in 1939 [2], in low-intensity alkaline-element spectra. Greater attention to them dates, however, from Garton and Tomkins's high-resolution intense spectra in 1969, which revealed the evolution of barium Rydberg series into quasi-Landau spectra extending 100 cm^{-1} beyond the ionization threshold, as shown in Fig. 1 [3]. Most features of Rydberg diamagnetism have since been interpreted qualitatively and then reproduced quantitatively in extreme detail by numerical diagonalization of the Hamiltonian (in a.u.) of a Rydberg electron

$$H=-\tfrac{1}{2}\nabla^2-\frac{1}{r}+\tfrac{1}{8}\omega_c^2 r^2\sin^2\theta \tag{1}$$

($\omega_c=$ cyclotron frequency) in a basis of orbitals $\{\psi_i\}$. [The last term of (1), the diamagnetic potential, represents the kinetic energy of the Larmor precession, which is not described by (1) explicitly.] The number of ψ_i utilized approaches 10^5 in the most recent successful comparison of theory and measurement for a Landau spectrum with resolution approaching 10^{-3} cm [4]. Calculations of this kind confirm the adequacy of the Hamiltonian (1) without providing any indication of the mecha-

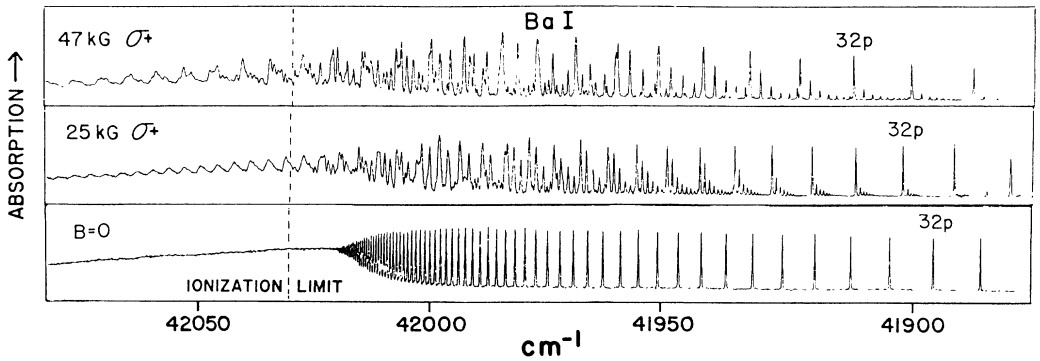

FIG. 1. Photoabsorption spectrum of barium near the ionization limit in magnetic fields B of different strengths (Ref. [3]).

nism responsible for the detailed and evolving structure of the spectra.

Note, for initial orientation, the gradual emergence of additional lines in the upper bank of Fig. 1, within each gap between lines denoted by np and $(n+1)p$, in the range $37 \geq n \geq 30$. These lines might be attributed at first to a breakdown of the selection rules that restricts the optical transitions from the ground state $6s$ of Ba to np levels; the angular anisotropy of diamagnetism affords optical excitation to all nl levels with odd l values. Further consideration of degenerate perturbation theory labels the set of additional lines to the right of np by nq, where q corresponds to one eigenvalue of the perturbation matrix $V^n_{ll'}$. This classification by indices (n,q) becomes less obvious in Fig. 1 as n approaches 40 and the sequences with different n start intermingling, but it has been pressed forward with success using sharper spectra and more elaborate calculations.

A new element of the Rydberg diamagnetism has emerged, however, with the advent of laser-spectroscopy-resolution spectra of atomic H excited with polarization orthogonal to **B**. Detailed classification of individual lines, by quasi-Landau labels that imply approximate separability of the Hamiltonian (1), was found to break down brusquely with increasing level energy, when this energy approaches the ionization threshold to within a small multiple of ω_c (~ 25 cm^{-1} at a field strength of ~ 6 T) [5]. The statistical distribution of level spacings, with the Poisson-like character associated with the occurrence of classification labels, turns at this point rapidly into the distribution associated with the absence of any classifying label and with the onset of classical chaos [5,6]. The quasi-Landau spectral structures above the ionization threshold clearly represent autoionization energy levels, being degenerate with continua of Landau levels to which they are coupled by the central field prevailing at short radial distances. An early calculation of classical orbits starting at large r and $\theta \simeq 90°$ and governed by the Hamiltonian (1) had in fact shown them to escape eventually along the **B** axis [7]. Nevertheless the discovery of Ref. [5] has spurred extensive studies of classical orbits governed by (1), chaotic or quasichaotic, rather than inquiries into the circumstances of atomic mechanics responsible for that phenomenon.

It is in fact well known that any one level of a multichannel spectrum of excitations can be classified as pertaining to a single channel—a quasi-Landau channel in our case—only when the spacing of nearby levels in all interacting channels is sufficiently large [8]. ("Channel interactions" imply exchanges of energy and/or angular momentum between an excited electron and an atomic or molecular core, changes that are described as transfers of the system from one channel to another and occur generally at short radial distances.) The circumstances of Ref. [5] indicate accordingly that the spectral evolution shortly below the ionization threshold marks the limit above which individual levels can no longer be assigned to any single channel. The observed position of this limit appears plausible because the spacing of the lower Landau levels converges there to its zero value, characteristic of each of the series limits lying just above the zero-field ionization threshold. These points have been made in Ref. [9] and illustrated with a model treatment. The limit energy could not be evaluated at that time for lack of quantitative information on the channel interaction that prevails at short radial distances among all the Landau and quasi-Landau channels. A more advanced model treatment, yet also short of input data, has served quite recently to interpret the striking effects of interactions *among* Landau channels described in Ref. [4] [10]. Adequate input data have then been provided for a strong-field example ($B \simeq 10^3 - 10^4$ T) using an R matrix with radius ≤ 100 a.u. and a basis set of $< 10^3$ functions; the results demonstrate that quasi-Landau excitations appear as interlopers of the Landau spectrum just above the ionization threshold [10]. The immediate goal of the present paper is to develop a quantitative treatment of the interactions among all Landau and quasi-Landau channels.

A curious feature of this task, common to the treatment of most multichannel phenomena, is that a rather extensive assignment of spectral levels to specific channels is afforded for phenomena governed by *nonseparable* Hamiltonians. Indeed interest in the diamagnetism of Rydberg spectra has been enhanced by viewing (1), after trivial separation of the φ coordinate, as the simplest prototype nonseparable Hamiltonian in the coordinate pair (r,θ). Our task should thus deal with an approximate separation of coordinates, presumably localized in restricted ranges of their variation. An important tool for this purpose has long been made available by Seaton [8]. One integrates a multichannel Schrödinger equation outwards from a center of mass, delaying any consideration of boundary conditions at infinite distance. Thereby the problem becomes more nearly separable. Belated imposition of the boundary conditions enforces then the nonseparability through a transparent procedure of linear algebra [11]. Further analysis has been provided by R-matrix procedures that confine the diagonalization of complex Hamiltonians to the volume of an atomic or molecular core and are complemented by semianalytic wave functions at longer ranges [4,10].

The R-matrix approach is, however, inappropriate to the Rydberg diamagnetism, or other effects, which warp the spherical symmetry progressively at increasing radial distances rather than within a core region. A novel procedure to deal with this circumstance will be introduced qualitatively in Sec. II. Its analytical development and an initial numerical application will follow in Secs. III and IV with fuller implementation deferred to later papers.

Part of the recent interest in Rydberg diamagnetism stemmed from viewing it as a prototype for more complex nonseparable problems, as noted above. The procedures to be introduced in this paper turn out to be equally relevant throughout atomic and molecular physics, all of whose spectral and collision problems are cast in a single mold by use of hyperspherical coordinates [12]. Expansion into hyperspherical harmonics replaces then all coordinates but one with sets of quantum numbers that characterize the *shape* of the system and its channels of fragmentation or excitation. The adiabatic procedure of integration of the hyperspherical Hamiltonian suggested in Ref. [12] has proved, however, inade-

quate to account for the description of resonances in high potential regions without excessive numerical labor, owing to its initial disregard of radial-angular correlations. These correlations can now be included at the outset by expansion into (hyper)spherical harmonics from which resonances at high potentials emerge automatically [13]. The procedure to be introduced in the following section is equally applicable to spherical and hyperspherical expansions, as will be indicated by parenthetical remarks in the following sections.

II. THEORETICAL FRAMEWORK

Spectra of nonseparable systems display rather surprising evidence for particle concentration in regions of high potential energy, as in the quasi-Landau states of diamagnetism and in its analogs in multiparticle systems [3,14]. Reference [13] has identified the mechanism for this concentration in the diagonalization of the relevant *finite* Hamiltonian matrix. Eigenvectors localized in regions of highest and lowest potential energy, with highest- and lowest-energy eigenvalues, are represented in Ref. [13] as superpositions of the *same small set of low-l orbitals,* orthogonalized by a switch from uniform to alternate sign. Localization at low potentials is familiar; orthogonalization of a finite basis combines with the mutual repulsion of eigenvalues of finite matrices to generate a corresponding localization at high potential.

This localization hinges, of course, on specific properties of the Hamiltonian. The matrix of Ref. [13] is tridiagonal with off-diagonal elements that couple higher-l orbitals more weakly than those of low l. Strongly coupled low-l orbitals serve then to construct the eigenvectors with lowest and highest energy.

The relevance of restricting the size of the Hamiltonian matrix becomes apparent by contrasting the results of Ref. [13] with those of earlier adiabatic treatments of diamagnetic and analogous Hamiltonians [15]. The adiabatic procedure works out the angular dependence of the wave function at each radial distance without reference to angular-radial correlations, thus effectively allowing unrestricted admixture of high-l harmonics. Wave functions orthogonal to low-energy states could then be constructed from this infinite basis of harmonics without forcing their localization at high potentials. The observed localization would thus be achieved only through laborious nonadiabatic corrections [16].

In Ref. [13] the use of a finite basis of harmonics resulted from its treating the diamagnetic potential as a perturbation of the degenerate manifold of hydrogenic states with equal quantum number n and with spherical harmonics $Y_{lm}(\theta,\varphi)$, $l<n$. We proceed here to show how the restriction to a finite set of harmonics flows instead from the dynamics of the Hamiltonian (1).

A. Dominance and decline of the centrifugal field

The dependence of the Hamiltonian (1) on the angular coordinates (θ,φ) is replaced by its dependence on quantum numbers (l,m) through the unitary transformation matrix of harmonics $Y_{lm}(\theta,\varphi)\equiv(\theta,\varphi|lm)$, yielding

$$H=-\frac{1}{2}\frac{d^2}{dr^2}+\frac{l(l+1)}{2r^2}-\frac{1}{r}+\frac{1}{8}\omega_c^2 r^2(lm|\sin^2\theta|l'm)$$
$$=H_{0l}+\tfrac{1}{8}\omega_c^2 r^2(lm|\sin^2\theta|l'm)\ . \qquad (2)$$

This representation of the Hamiltonian in the independent variables l and r isolates the influence of the centrifugal field in the single term $l(l+1)/2r^2$, whose magnitude increases with l and declines with increasing r. Casting the problem in the (l,r) variables helps to illustrate how the dynamical influence of the centrifugal field focuses the diamagnetic action onto a subset of lower-l harmonics.

This focusing emerges even in the absence of a magnetic field when (2) reduces to the Coulomb field Hamiltonian H_{0l} diagonal in l. The decline of the centrifugal term of (2) with increasing r gives way here to dominance of the Coulomb term $-1/r$. Energy-normalized radial eigenfunctions of H_{0l} are conveniently represented in terms of the Milne phase $\phi_l(r)$ [17] as

$$f(r)=\alpha_l(r)\sin\phi_l(r),\quad \alpha_l(r)=\left[\frac{2}{\pi\dfrac{d\phi_l}{dr}}\right]^{1/2}. \qquad (3)$$

Figure 2 plots this phase, evaluated for a sequence of (even) l values and for the zero eigenvalue of H_{0l}, boosted by $l\pi$ at $r=0$ so as to converge to a value common to all l as $r\to\infty$. The flatness of all $\phi_{l\neq 0}$ at low r reflects the suppression of any phase increase by the centrifugal barrier. Phase growth sets in as r approaches $l(l+1)/2$ and leads rapidly to insertion of $\phi_l(r)$ into the bundle of curves converging toward the $\sqrt{8r}$ course of $\phi_0(r)$. Figure 2 thus suggests that the transition of the whole diamagnetic Hamiltonian away from dominance of the centrifugal field might also prove rapid.

Note that the combined centrifugal plus Coulomb potential, $l(l+1)/2r^2-1/r$, turns negative at $r=l(l+1)/2$ and bottoms out at $r=l(l+1)$. The locus $r=l(l+1)/2$ marks the boundary from centrifugal to Coulomb dominance. The latter locus, indicated in Fig. 2 by a *curved*

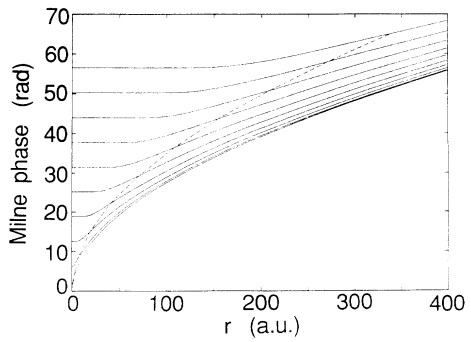

FIG. 2. Phase function $\phi_l(r)$ of eigenfunctions of the Coulomb operator H_{0l} [Eq. (2)] with $E=0$ in the Milne form. Each ϕ_l, defined modulo π, has been set at $l\pi$ at $r=0$, thus ensuring that all ϕ_l coincide as $r\to\infty$. The dashed line marks the lower-r bound of the region of approximate separability.

boundary line, marks the onset of an asymptotic range where phase and amplitude can be expanded into powers of $l(l+1)/r$. The absence in Fig. 2 of curves with odd-l values reflects the separability of the Hamiltonian (2) into submatrices with even and odd l, due in turn to the identity $\sin^2\theta=\sin^2(\pi-\theta)$. (Even l will be assumed in the following, for brevity, unless otherwise stated.)

We shall view the main role of the diamagnetic potential in Eq. (2) as that of mixing Coulomb functions with different l through the action of its off-diagonal elements. Specifically these elements mix only for $|l-l'|=2$ because the matrix of $\sin^2\theta$ is tridiagonal, here as in Ref. [13]. The mixing is effective at any given r, of course, only to the extent that the Coulomb functions depart from zero significantly at that r, thus excluding those (l,r) regions where centrifugal dominance quenches Coulomb functions. Here we see how the diamagnetic action is effectively confined at any given r to the finite set of l components lying below, or modestly above, the *curved boundary* drawn in Fig. 2.

[Centrifugal dominance and the curved boundary are also apparent in atomic and molecular phenomena free of diamagnetism, particularly so when viewed in hyperspherical coordinates [12]. In the hyperspherical Hamiltonian analogous to (2), the usual radial variable r is replaced by an inertial radius R and the orbital number l by a "grand angular momentum" number λ. The complicated set of Coulomb interactions among electrons and nuclei remains inversely proportional to R, but the effective atomic number—unity in (2)—turns into a matrix $C_{\alpha\alpha'}$ that does not commute with λ, thus playing a role corresponding to that of the diamagnetic term of (2). The Hamiltonian has thus the form

$$\frac{1}{2M}\left[-\frac{d^2}{dR^2}+\frac{[\lambda+(3N-5)/2]^2-\frac{1}{4}}{R^2}\right]-\frac{C_{\alpha\alpha'}}{R}\ , \quad (4)$$

for an aggregate of N particles with total mass M. The transition from dominance of the centrifugal field to that of Coulomb interactions is then controlled by the effective ratio of the noncommuting centrifugal and Coulomb terms of (4).]

B. The onset of diamagnetism

The diamagnetic potential in Eq. (2) is much weaker than the centrifugal and Coulomb terms for r values on the order of 100 a.u. and B values ≤ 10 T, i.e., of laboratory strengths. (Fields of astrophysical strengths are overwhelming at lower r, posing problems altogether different from those considered here.) A major influence of diamagnetism emerges nevertheless wherever centrifugal dominance in the lth channel gives way to dominance of the Coulomb field which commutes with the diamagnetic potential. The orbital parameter l ceases here to be a *good* quantum number, allowing unrestricted mixing of the lth wave function (3) with lower-l functions.

We face thus the task of tracing the evolution of wave functions $\psi_{l_0}(r,\theta,\varphi)$, each of them identified at $r\ll l_0(l_0+1)$ by its angular dependence $Y_{l_0m}(\theta,\varphi)$ and by its radial dependence $\propto r^{l_0+1}$. (The magnetic number m remains "good" at all r.) This function will be represented at larger r as a superposition of components with different l values,

$$\psi_{l_0}(r,\theta,\varphi)=\sum_l Y_{lm}(\theta,\varphi)F_{ll_0}(r),$$
$$F_{ll_0}(r)\to\frac{2^{2l_0+1}}{(2l_0+1)!}r^{l_0+1}\delta_{ll_0}\ \text{ as } r\to 0\ . \quad (5)$$

The mixing of l components by the magnetic field also modifies the phase of each l component, whereby $F_{ll_0}(r)$ no longer remains proportional to the regular Coulomb function (3) but is represented by

$$F_{ll_0}(r)=\alpha_l(r)[\sin\phi_l(r)a_{ll_0}(r)+\cos\phi_l(r)b_{ll_0}(r)]\ . \quad (6)$$

The ratio $b_{ll_0}(r)/a_{ll_0}(r)$ equals the tangent of the phase shift imposed upon the lth component of (4). The modulus of the pair $\{a_{ll_0},b_{ll_0}\}$ represents instead the amplitude of this component.

Casting $F_{ll_0}(r)$ in its form (6) diagonalizes the Coulomb term H_{0l} of the Hamiltonian (2). The residual, diamagnetic and nondiagonal, term of (2) will then be "dressed" in Sec. III, by factors analogous to (6) that quench it in the ranges (l,r) of centrifugal dominance. The rise of these factors accompanying the centrifugal decline will then induce seemingly erratic oscillations of the diamagnetic effect to be displayed in Sec. IV.

The evolution of the set of functions (5) through the onset of diamagnetism will be described in Sec. III by adapting and complementing a semianalytic phase-amplitude treatment that was developed in the 1960s [18] but does not appear to have been utilized in the meantime. The thrust of Ref. [18(a)] is to identify linear superpositions of eigenfunctions F_{ll_0} on which the diamagnetic action is variationally stable. That is, one construct at each radial distance eigenchannels of the diamagnetic potential characterized by a phase shift $\delta_p(r)$ common to all components $F_{ll_0}(r)$; the value of each δ_p measures the effective strength of diamagnetism in the pth channel, accumulated in the range $0<r'\leq r$. The wave function of each eigenchannel, at any given radial distance r, can be represented as a superposition of eigenfunctions $F_{ll_0}(r)$ of the Hamiltonian (2) with different initial orbitals l_0,

$$f_p(r,l)=\sum_{l_0}F_{ll_0}(r)B_{l_0p}(r)$$
$$=\alpha_l(r)\sin[\phi_l(r)+\delta_p(r)]C_{lp}(r)\ . \quad (7)$$

The dependence of the coefficients B_{l_0p} and C_{lp} on the radial distance r in Eq. (7) implies that the superposition of eigenfunctions $F_{ll_0}(r)$ varies in each interval $(r,r+dr)$ to encompass the additional contribution of diamagnetism in that interval. Accordingly each function $f_p(r,l)$ does *not* represent an eigenfunction of the Hamiltonian (2).

The analytical development of this procedure in Sec. III and its numerical implementation in Sec. IV for the Rydberg diamagnetism of the H atoms form the core of the present paper. A main element of the eigenfunction evolutions consists of numerous *level crossings,* that is, of

phase degeneracies of two functions yielding amplitude transfers between them. Their aggregate effect will provide the desired matrix of interaction parameters between observable excitation channels. Specifically, Sec. III will describe how to calculate the eigenvalues of eigenvectors of a reaction matrix $K(r)$, denoted as a "short-range K matrix" in Ref. [19] and equivalent to an R matrix. Its semianalytic procedure, implemented numerically in Sec. IV, displays the evolution of eigenvalues and eigenvectors as r increases, thus depicting the mechanism of wave-function propagation which remained obscure in earlier procedures. Transformation of the K matrix to the basis of "fragmentation channels," to be introduced in Sec. II D, provides the input for the calculation of transitions among Landau and quasi-Landau states by Seaton's multichannel quantum-defect theory [8] which was outlined in Ref. [9] and reported extensively in Ref. [19].

The opportunity of identifying a complete orthogonal set of eigenfunctions of an atomic or molecular Hamiltonian at its center of mass and of following its evolution to ionization or dissociation has long been apparent. Reference [12] stressed this opportunity, recalling from Ref. [20] that the expansion of $F_{ll_0}(r)$ at $r\to\infty$ into exponentials of r provides the elements of a pair of Jost matrices $J^{\pm}_{ll_0}$ that encompass all collision and spectral data of interest. The most critical part of the evolution of the set $\{\psi_{l_0}\}$, Eq. (5), appears to center in the band of the (l,r) space astride the curved boundary in Fig. 2, which is to be described in Secs. III and IV. The remainder of the evolution, at larger r values, will probably prove less critical, as anticipated by introductory discussions in the remainder of Sec. II.

[Multiparticle systems also display channel interactions that presumably stem principally from amplitude transfers among hyperspherical eigenfunctions in the range of parameters where the centrifugal dominance subsides. The centrifugal quantum number l is replaced, of course, by the grand angular momentum number λ. The higher dimensionality of hyperspherical bases complements λ with additional sets of quantum numbers indicated globally in Eq. (4) by the index α of the Coulomb matrix $C_{\alpha\alpha'}$. Alternative incompatible sets α, analogous to those of alternative angular momentum couplings, prove relevant, e.g., at the limit of minimal inertial radius, $R\to 0$, as anticipated on p. 48 of Ref. [21], and at the opposite limit, $R\to\infty$, where different sets label different fragmentations of the system.]

C. The range of approximate separability

Once the centrifugal dominance has subsided for a set of lower-l values, $0\le l\le L$, the corresponding phase $\{\phi_l(r)\}$ grow smoothly with r, as shown in Fig. 2 well on the right of the curved boundary. A steady state should prevail in this range of the (r,l) variables affording the approximate separability of the Hamiltonian (2) that is suggested by the pattern of the spectra of Fig. 1 for $n>30$ and of the spectra of Fig. 3 calculated for a broad range of n in Ref. [13]. Eigenfunctions represented in appropriate coordinates should display the localization in l derived in Ref. [13]. Figure 3 shows that the eigenvalue spectrum preserves a constant pattern as n increases; the pattern of localization in the scaled variable $l/\sqrt{r}$ is also preserved.

Note at the outset that the fixed-n eigenvectors of Ref. [13] differ from the fixed-r eigenvectors characterized in Sec. II B by a phase shift $\delta_p(r)$ common to all their harmonic components (6): Corresponding antinodes of hydrogenic radial functions with equal n and different l spread over a sizable range of r values [22], whereas the components (6) are superposed at equal r. Indeed the Hamiltonian (2) does not display the features of the fixed-n Hamiltonian of Ref. [13] that have been indicated as critical in the first paragraph of Sec. II. Eigenvectors of (2) calculated by R matrix on a fixed-r surface display only a limited localization [23]; this result is understandable since the phase $\phi_l(r)$ of their components (6) range over several quadrants.

Separable wave functions of a pair of variables (x,y) are generally represented as $f(x)g(y)$. Anticipating only

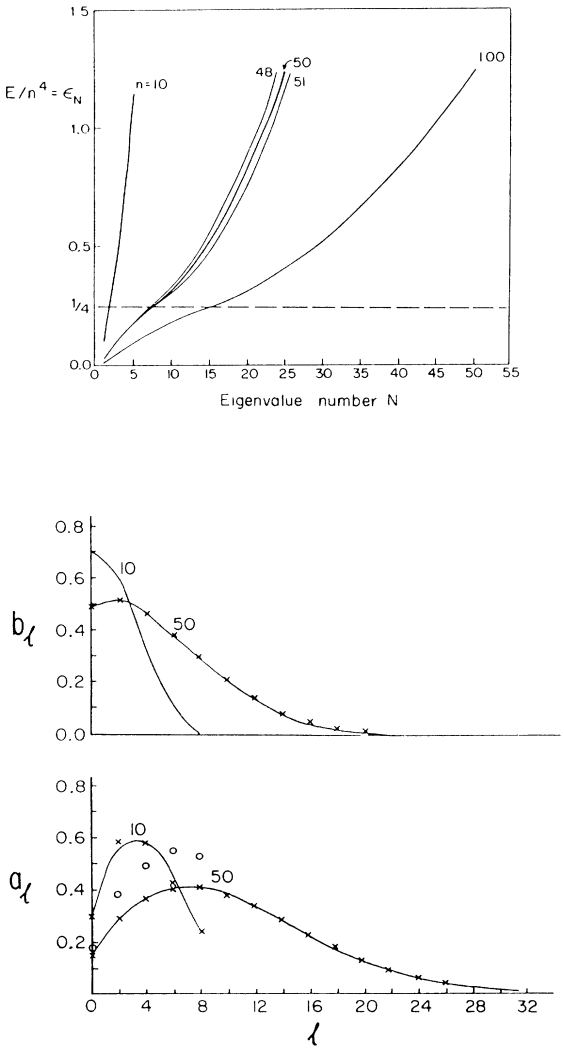

FIG. 3. Eigenvalues ε_N and eigenvectors $\{a_l,b_l\}$ of the diamagnetic Hamiltonian within hydrogenic shells with principal quantum numbers $N\equiv(10,50,100)$, from Ref. [13].

approximate separability we shall use the notation $f(x)g(x;y)$ to indicate that $g(y)$ may depend parametrically, i.e., weakly, on x. The construction of quasiseparable eigenfunctions, to be reported in a separate paper, is expected to proceed as follows. Recall that Sec II B dealt with a short-range K matrix to be constructed and diagonalized on successive lines $r=$const of the (r,l) plane. We anticipate here the construction of a set of quasiseparable wave functions of the form

$$\chi_q(r,l)=\sin\phi_q(r,l)g_q(\phi_q;l) \ . \tag{8}$$

The phase ϕ_q replaces here the coordinate r of Sec. II B insofar as wave fronts of (8) are represented by curves $\phi_q(r,l)=$const of the (r,l) plane in contrast to the straight lines $r=$const over which the phase shifts $\delta_q(r)$ and coefficients $B_{l_0p}(r)$ of Eq. (7) remain constant. In further contrast to Sec. II the functions $\chi_q(r,l)$ are to be eigenfunctions of the Hamiltonian (2), whereas the $f_p(r,l)$ of Eq. (7) are not. The construction of eigenfunctions (8) defined over a limited portion of the (r,l) plane—i.e., on the right of the curved boundary line in Fig. 2—appears to present a novel challenge.

D. The asymptotic range: Fragmentation channels

In the limit of $r\to\infty$ the wave fronts $\phi_q(r,l)=$const for eigenfunctions $\chi_q(r,l)$ of the Landau or quasi-Landau type—i.e., localized in the (r,θ) plane astride the axes $\theta=0°$ or $\theta=90°$—should reduce to $r\cos\theta=$const or $r\sin\theta=$const, respectively. Whether or not this requirement will be met automatically, by extending the formulation outlined in Sec. II C to a larger-r limit, remains to be determined. In the positive case the sets of states represented by the eigenfunctions (8) constitute the "fragmentation channels." (See, e.g., Chap. 7 of Ref. [19].) In the negative case, a further transformation of the eigenfunctions $\chi_q(r,l)$ will be required to represent the fragmentation channels.

III. PROPAGATION OF THE RADIAL FUNCTIONS $F_{ll_0}(r)$

The radial eigenfunctions $F(r)$ of the Hamiltonian (2) with energy eigenvalue E defined by Eqs. (4) and (5) are governed by the Schrödinger equation

$$\sum_{l'}[(H_{0l}-E)\delta_{ll'}+\beta r^2U_{ll'}]F_{l'l_0}(r)=0 \tag{9}$$

where

$$\beta=\tfrac{1}{16}\omega_c^2, \quad U_{ll'}=v_l\delta_{ll'}+w_{l\pm1}\delta_{l'=l\pm2} \ ,$$
$$v_l=1-[4l(l+1)-3]^{-1} \ , \tag{9'}$$
$$w_{l\pm1}=-\tfrac{1}{2}[1-(2l+1\pm2)^{-2}][1-(l+\tfrac{1}{2}\pm1)^{-2}]^{-1/2} \ .$$

The nonzero matrix elements of $\sin^2\theta$ converge to 1 and $-\frac{1}{2}$, respectively, as l increases, thus reproducing one feature of the matrix that yields the eigenvector localizations in Ref. [13]. The structure (6) of $F_{ll_0}(r)$ ensures that $(H_{0l}-E)F_{ll_0}$ in (9) reduces to the propagation of the coefficients $\{a_{ll_0}(r),b_{ll_0}(r)\}$, which is thus contributed by the cumulative action of the matrix $\beta r^2U_{ll'}$ combined with the propagation of the Coulomb field functions $\{\alpha_l\sin\phi_l,\alpha_l\cos\phi_l\}$. The following evaluation of this contribution mirrors the treatment of Ref. [18(c)]; it is well known in atomic mechanics but will be presented sequentially in some detail.

A. Propagation of the amplitudes $\{a_{ll_0}(r),b_{ll_0}(r)\}$

The contribution to $\{\alpha_{ll_0}(r),b_{ll_0}(r)\}$ from the matrix $\beta r^2U_{ll'}$, over a radial interval dr' is propagated from r' to r by the Green's function of $H_{0l}-E$,

$$G_l(r,r')=\pi\alpha_l(r)\alpha_l(r')\sin[\phi_l(r)-\phi_l(r')] \ , \tag{10}$$

which is identified by its behavior at $r'=r$,

$$G_l(r,r)=0 \ , \tag{10a}$$

$$\frac{d}{dr}G_l(r,r')|_{r'=r}=2 \ , \tag{10b}$$

and has the property relevant to us

$$(H_{0l}-E)\int_0^r dr'G_l(r,r')f(r')=-f(r) \ . \tag{11}$$

To verify Eq. (11) note that, whereas direct application of $(H_{0l}-E)$ to $G_l(r,r')$ yields no contribution, one may split the $-\frac{1}{2}(d/dr)^2$ term of H_{0l} by applying first d/dr to $G_l(r,r')$ and then the residual $-\frac{1}{2}d/dr$ to the limit of integration in (11), whence (10b) yields just the right side of (11).

Equation (11) serves now to represent $F_{ll_0}(r)$ as the sum of the regular eigenfunction (3) of H_{0l} and of the contribution of the diamagnetic potential $\beta r'^2\sum_{l'}U_{ll'}F_{l'l_0}(r')$ integrated over r' and propagated from r' to r by the Green's function $G_l(r,r')$,

$$F_{ll_0}(r)=\alpha_l\sin\phi_l(r)+\int_0^r dr'G_l(r,r')\beta r'^2\sum_{l'}U_{ll'}F_{l'l_0}(r') \ . \tag{12}$$

Upon entering this expression in Eq. (9), the operator $H_{0l}-E$ wipes out the $\alpha_l\sin\phi_l$ term of F_{ll_0} and reduces its integral term to $-\beta r^2\sum_{l'}U_{ll'}F_{l'l_0}(r)$ thus cancelling the second term of Eq. (9).

Returning now to the expression (6) of $F_{ll_0}(r)$ in terms of the coefficients $\{a_{ll_0},b_{ll_0}\}$, we see that Eq. (12) amounts to setting in (6)

$$a_{ll_0}(r)=1+\pi\int_0^r dr'\alpha_l(r')\cos\phi_l(r')\beta r'^2\sum_{l'}U_{ll'}F_{l'l_0}(r') \ , \tag{13a}$$

$$b_{ll_0}(r)=-\pi\int_0^r dr'\alpha_l(r')\sin\phi_l(r')\beta r'^2\sum_{l'}U_{ll'}F_{l'l_0}(r') \ . \tag{13b}$$

Instead of solving Eq. (9) we have thus actually replaced it by a system of coupled integral equations in $\{a_{ll_0},b_{ll_0}\}$.

This system is, however, easily accessible to numerical solution since a simple differentiation reduces it to the system of coupled first-order equations,

$$\frac{da_{ll_0}}{dr}=\pi\beta r^2\sum_{l'}(L_{ll'}^{(aa)}a_{l'l_0}+L_{ll'}^{(ab)}b_{l'l_0}) , \tag{14a}$$

$$\frac{db_{ll_0}}{dr}=\pi\beta r^2\sum_{l'}(L_{ll'}^{(ba)}a_{l'l_0}+L_{ll'}^{(bb)}b_{l'l_0}) , \tag{14b}$$

with

$$\begin{aligned}
L_{ll'}^{(aa)}&=\alpha_l(r)\cos\phi_l(r)U_{ll'}a_{l'}(r)\sin\phi_{l'}(r) ,\\
L_{ll'}^{(ab)}&=\alpha_l(r)\cos\phi_l(r)U_{ll'}\alpha_{l'}(r)\cos\phi_{l'}(r) ,\\
L_{ll'}^{(ba)}&=-\alpha_l(r)\sin\phi_l(r)U_{ll'}\alpha_{l'}(r)\sin\phi_{l'}(r) ,\\
L_{ll'}^{(bb)}&=-\alpha_l(r)\sin\phi_l(r)U_{ll'}\alpha_{l'}(r)\cos\phi_{l'}(r) .
\end{aligned} \tag{14c}$$

The matrix $L_{ll'}$, Eq. (14c), represents the diamagnetic potential $\beta r^2U_{ll'}$ "dressed" by Coulomb field eigenfunctions, as anticipated in Sec. II. This matrix may also be viewed as equivalent, in our real representation, to a complex matrix $\exp(iH_{0l}r)V_{ll'}\exp(-iH_{0l'}r)$ of the type that familiarly represents a perturbation in the *interaction picture*. Numerical solution of Eqs. (14) appears feasible but not very apt to provide physical interpretation. It may serve nevertheless to check the results of the following approach.

See *Note added in proof* at the end of the paper.

B. Eigenchannels of phase shift

The process of solving the system (14) numerically could extend, in principle, over the whole range of r even though it is more effective in the range $r\sim l(l+1)$ where $|l_0-l|$ remains small. However, one does not readily see how to draw from it the formation of states localized in regions of high or low potential, or—more immediately—how to take advantage of the smooth trend of the phases $\phi_l(r)$ at large r. A physically meaningful stepping stone toward these goals has been introduced in Ref. [18(a)]. One identifies at each r linear superpositions of solutions $F_{ll_0}(r)$ for which the diamagnetic potential has added *an equal shift* δ_p to all the relevant Coulomb phases ϕ_l. The physical meaning of this selection becomes apparent by imagining the diamagnetic action as truncated at the given r: in this case δ_p would represent the entire non-Coulomb phase shift observable through elastic collisions of an electron with the field thus truncated. (The study of phenomena involving a field truncated at alternative radial distances r belongs to the mathematical procedure called *invariant imbedding* [24].)

Each *eigenphase shift* δ_p is identified and evaluated as the arctangent of an eigenvalue of the reaction matrix $K_{ll'}$ whose calculation amounts to solving the system (14) by an alternative procedure. Notice initially that a solution of Eq. (9) in terms of the K matrix is represented by multiplying the expression (6) of $F_{ll_0}(r)$ with the reciprocal of the coefficient matrix a_{ll_0},

$$\sum_{l_0}F_{ll_0}(r)(a^{-1})_{l_0l'}=\alpha_l(r)\left[\sin\phi_l(r)\delta_{ll'}+\cos\phi_l\sum_{l_0}b_{ll_0}(a^{-1})_{l_0l'}\right] . \tag{15}$$

Inspection of this equation identifies the coefficient of $\cos\phi_l$ as the reaction matrix

$$K_{ll'}(r)=\sum_{l_0}b_{ll_0}(a^{-1})_{l_0l'} . \tag{16}$$

Applying the same transformation to (14) yields the intermediate equations,

$$\begin{aligned}
&\sum_{l_0}\frac{da_{ll_0}}{dr}(a^{-1})_{l_0l'}\\
&\quad=\pi\beta r^2\alpha_l(r)\cos\phi_l(r)\\
&\qquad\times\sum_{\lambda}U_{l\lambda}\alpha_\lambda(r)[\sin\phi_\lambda(r)\delta_{\lambda l'}+\cos\phi_\lambda(r)K_{\lambda l'}] ,
\end{aligned} \tag{17a}$$

$$\begin{aligned}
&\sum_{l_0}\frac{db_{ll_0}}{dr}(a^{-1})_{l_0l'}\\
&\quad=-\pi\beta r^2\alpha_l(r)\sin\phi_l(r)\\
&\qquad\times\sum_{\lambda}U_{l\lambda}\alpha_\lambda(r)[\sin\phi_\lambda(r)\delta_{\lambda l'}+\cos\phi_\lambda(r)K_{\lambda l'}] .
\end{aligned} \tag{17b}$$

It should be stressed here that the multiplication by $(a^{-1})_{l_0l'}$ introduces singularities in Eqs. (15)–(17) wherever the $\det|a_{ll_0}|$ vanishes. These singularities are inherent in scattering theory and are often the loci of important parameters. For example, a pole occurs in the K matrix whenever an eigenphase shift transverses an odd multiple of 90°. Analogous poles may prove significant in the following.

Note next the structure of the gradient of Eq. (16),

$$\begin{aligned}
\frac{dK_{ll'}}{dr}&=\sum_{l_0}\left[\frac{db_{ll_0}}{dr}(a^{-1})_{l_0l'}+b_{ll_0}\left[\frac{d(a^{-1})}{dr}\right]_{l_0l'}\right]\\
&=\sum_{l_0}\left[\frac{db_{ll_0}}{dr}(a^{-1})_{l_0l'}-\sum_{\lambda}K_{l\lambda}\frac{da_{\lambda l_0}}{dr}(a^{-1})_{l_0l'}\right] .
\end{aligned} \tag{18}$$

The first term in the last brackets of (18) coincides with the left-hand side of Eq. (17b); the second term in the brackets consists of the matrix product of $-K_{l\lambda}$ and of the left-hand side of (17a). A single nonlinear first-order equation that determines $K_{ll'}$ results thus by equating (18) to the sum of the right sides of Eqs. (17b) and of (17a), the latter multiplied by $K_{l\lambda}$ on its left,

$$\begin{aligned}
\frac{dK_{ll'}}{dr}=&-\pi\beta r^2\sum_{\lambda\mu}\alpha_l(r)[\delta_{l\lambda}\sin\phi_\lambda(r)+K_{l\lambda}\cos\phi_\lambda(r)]\\
&\times U_{\lambda\mu}\alpha_\mu(r)[\sin\phi_\mu(r)\delta_{\mu l'}+\cos\phi_\mu(r)K_{\mu l'}] .
\end{aligned} \tag{19}$$

This basic result of Ref. [18] determines, in essence, the phase shifts generated by the diamagnetism, which are central to the phase-amplitude approach. The residual determination of amplitudes conjugate to phase shifts is treated in Ref. [18] for single channels only and will be extended here to our multichannel case.

Direct integration of Eq. (19), to yield the matrix $K_{ll'}$ as a function of r, proves unnecessary. Reference [18(a)] has designed a procedure that replaces (19) by equations that determine the eigenvalues $\tan\delta_p(r)$ and eigenvectors $\langle l|p(r)\rangle$ of $K_{ll'}$, parameters that are more instructive than $K_{ll'}$ itself. To this end, enter the expression

$$K_{ll'}(r)=\sum_p \langle l|p(r)\rangle \tan\delta_p(r)\langle p(r)|l'\rangle \tag{20}$$

in Eq. (19), and matrix-multiply the result by $\cos\delta_p\langle p(r)|l\rangle$ on its left and by $\langle l'|p'(r)\rangle\cos\delta_{p'}$ on its right. The resulting equation condenses into

$$\begin{aligned}&\frac{d\delta_p}{dr}\delta_{pp'}+\sin[\delta_p(r)-\delta_{p'}(r)]\sum_l \frac{d\langle p(r)|l\rangle}{dr}\langle l|p'(r)\rangle \\ &\quad=-\pi\beta r^2\sum_{l,l'}\langle p(r)|l\rangle\alpha_l(r)\sin[\phi_l(r)+\delta_p(r)]U_{ll'}\sin[\phi_{l'}(r)+\delta_{p'}(r)]\alpha_{l'}(r)\langle l'|p'(r)\rangle \\ &\quad\equiv\sum_{l,l'}\langle p(r)|l\rangle M_{ll'}^{(pp')}(r)\langle l'|p'(r)\rangle\ ,\end{aligned} \tag{21}$$

after utilizing the orthogonality relation

$$\sum_{l'}\frac{d\langle p(r)|l'\rangle}{dr}\langle l'|p'(r)\rangle + \sum_l\langle p(r)|l\rangle\frac{d\langle l|p\rangle}{dr}=\frac{d\delta_{pp'}}{dr}=0\ . \tag{22}$$

The transformation of Eq. (19) into (21) has condensed three separate physical elements into the single matrix kernel

$$\begin{aligned}M_{ll'}^{(pp')}=&-\pi\beta r^2\alpha_l(r)\sin[\phi_l(r)+\delta_p(r)] \\ &\times U_{ll'}\sin[\phi_{l'}(r)+\delta_{p'}(r)]\alpha_{l'}(r)\ ,\end{aligned} \tag{21'}$$

namely (1) the diamagnetic interaction $\beta r^2U_{ll'}$ from (9), (2) the *dressing* of this interaction by Coulomb radial functions $\{\alpha_l\sin\phi_l(r),\alpha_l\cos\phi_l(r)\}$, and (3) the phase shifting of these functions by the diamagnetic interaction accumulated throughout the range $0<r'<r$. [This last element replaces the occurrence of K on the right of (19).] Insertion of these diverse elements into a single matrix may prove convenient for the numerical integration procedure to be described in Sec. IV but raises a serious challenge for the interpretation of its results.

The diagonal and off-diagonal elements of Eq. (21) separate out neatly. The former afford direct evaluation of successive increments to each eigenphase shift $\delta_p(r)$. The latter afford the corresponding evaluation of the increment of each eigenvector component after a further two-step transformation: (a) division of (21) by $\sin[\delta_p(r)-\delta_{p'}(r)]$; (b) projection onto the eigenvector $\langle p'(r)|l'\rangle$, yielding

$$d\langle p(r)|l\rangle/dr=\sum_{p'(\neq p)}\left[\sum_{ll'}\langle p(r)|l\rangle M_{ll'}^{(pp')}\langle l'|p'(r)\rangle\right]\times\frac{\langle p'(r)|l'\rangle}{\sin[\delta_p(r)-\delta_{p'}(r)]}\ . \tag{23}$$

The operation (a) presents a problem in the event of near degeneracy of two eigenphases, $\delta_p(r)\sim\delta_{p'}(r)$. The resulting singularity, of a type frequent in atomic theory [25], will play a main role in Sec. IV.

C. The amplitude matrix

The recasting of the eigenfunction $F_{ll_0}(r)$, Eq. (6), in terms of the reaction matrix $K_{ll'}(r)$, in Eqs. (15) and (16), has factored out the amplitude coefficients $a_{ll_0}(r)$ and thereby part of the information content of Eq. (14a). We shall restore here this information, recasting $F_{ll_0}(r)$ once again as the superposition of eigencomponents characterized by eigenphases shifts δ_p and amplitude coefficients $A_{pl_0}(r)$.

With reference to Eqs. (15), (16), and (20), we write

$$\begin{aligned}F_{ll_0}(r)=&\alpha_l(r)\left[\sin\phi_l(r)\sum_p\langle l|p(r)\rangle\right. \\ &\left.+\cos\phi_l(r)\sum_p\langle l|p(r)\rangle\tan\delta_p(r)\right] \\ &\times\sum_{l'}\langle p(r)|l'\rangle a_{l'l_0} \\ =&\sum_p\alpha_l(r)\sin[\phi_l(r)+\delta_p(r)]A_{pl_0}(r)\ ,\end{aligned} \tag{24}$$

with

$$A_{pl_0}(r)=\frac{1}{\cos\delta_p(r)}\sum_{l'}\langle p(r)|l'\rangle a_{l'l_0}(r)\ . \tag{25}$$

We shall construct here an equation for $A_{pl_0}(r)$, combining the three separate equations for its factors $\{1/\cos\delta_p,\langle p(r)|l'\rangle,a_{ll_0}(r)\}$, namely, in essence, the diagonal portion of Eqs. (21), (23), and (14a), with $b_{ll_0}(r)$ represented as $\sum_{l'}K_{ll'}(r)a_{l'l_0}$.

All three terms of the equation will be cast conveniently in terms of the matrix $M_{ll'}^{(pp')}$ defined by Eq. (21), complemented by adjustments appropriate to each term. This procedure yields

The factor $\sin(\delta_p-\delta_{p'})$ in the denominator of (23) reduces similarly to $\delta_p(r)-\delta_{p'}(r)$, which is on the order of $\beta r^{7/2}$.

A. Eigenphase shifts

The complete set of calculated eigenphase shifts is presented in Fig. 6(c), for a field strength $B=5$ T, $r\leq 200$ a.u., and $E=0$ in Eq. (9). In this range the ratio of the diamagnetic and Coulomb potentials remains $\leq 10^{-4}$, and only ten phase shifts become appreciable on the vertical scale of Fig. 6(c). Figure 6(a) shows the first four non-negligible eigenphase shifts emerging from the centrifugal barrier on an enlarged scale, $r\leq 25$; Fig. 6(b) shows the first seven shifts for $r\leq 70$ a.u.

These figures display a complicated network of avoided crossings; all the intersections are actually avoided as no crossing is compatible with the pole singularity of Eq. (23). This large, seemingly surprising, amount of channel interaction stems from the commutability of diamagnetic

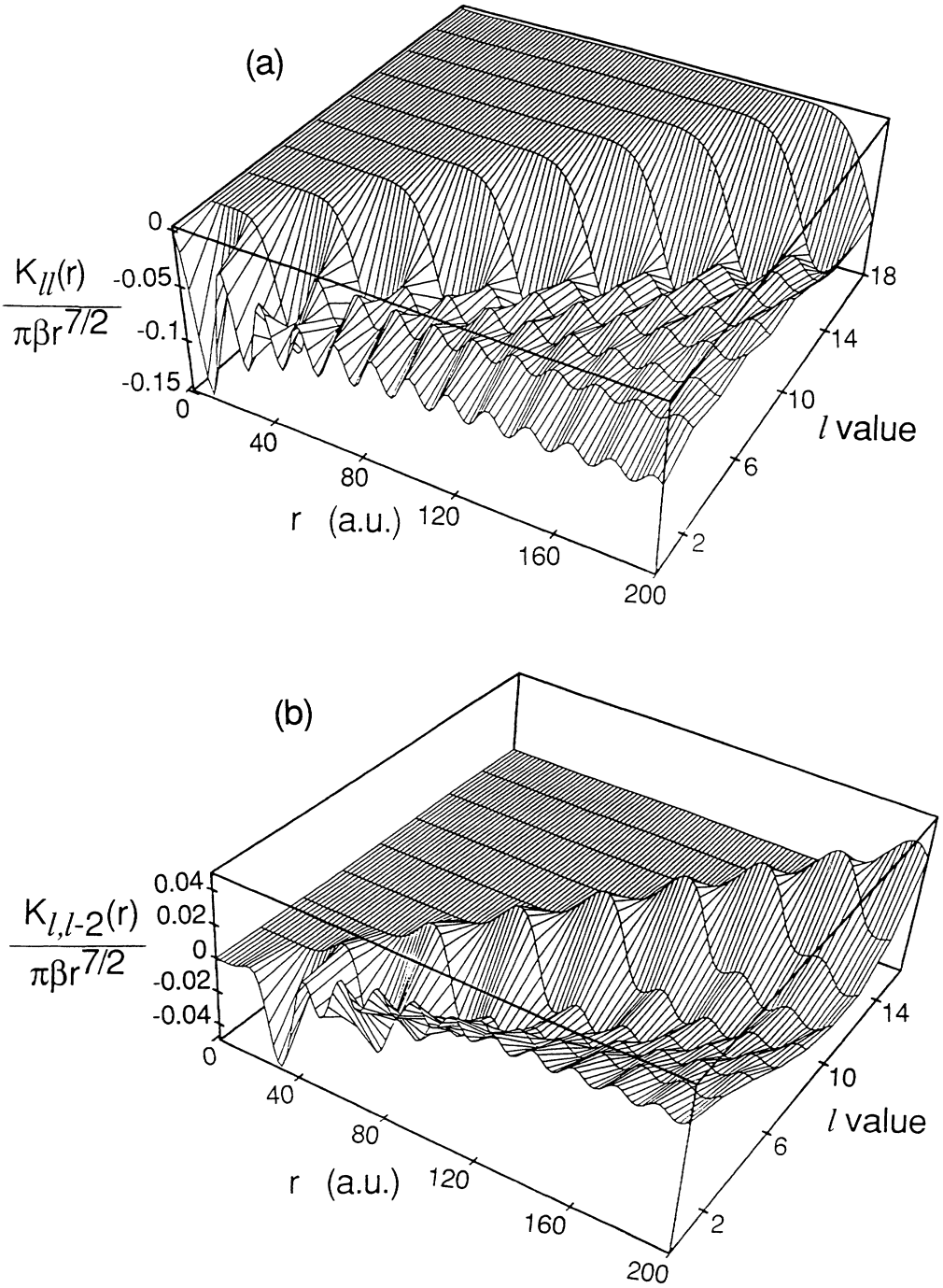

FIG. 5. Dependence on (r,l) of (short-range) reaction matrix elements: (a) $K_{ll}(r)$ and (b) $K_{l\,l-2}(r)$, in units of $\pi\beta r^{7/2}$.

the integral of the coefficient in Eq. (14), $\sim\beta r^3$, remains $\ll 1$ up to radial distances of several hundred a.u. In this range the solutions a_{ll_0}, b_{ll_0} depart but little from their initial values $(\delta_{ll_0}, 0)$ and the reaction matrix $K_{ll'}(r)$ remains $\ll 1$. The *eigenvectors* $\langle l|p(r)\rangle$ of $K_{ll'}$ depart nevertheless significantly from their initial values $\delta_{lp(0)}$, because the denominator in Eq. (23) is of the same order as its numerator. [A corresponding analysis of Eq. (31) shows that the amplitude factor $A_{pl_0}(r)$ coincides, to lowest order in ω_c^2, with the eigenvector $\langle p(r)|l_0\rangle$. The relationship $A_{pl_0}(r)\sim\langle p(r)|l_0\rangle$ in this weak-field range reflects the small value of the off-diagonal $(l\neq l_0)$ components of the eigenfunctions $F_{ll_0}(r)$, Eq. (6).]

To lowest order in ω_c^2, the right-hand side of the differential Eq. (23) for $K_{ll'}(r)$ reduces to the expression $-\pi\beta r^2 L_{ll'}^{(ba)}$ from (14c). This approximate form of (23) is readily integrated numerically, thus anticipating and illustrating a part of the results to be presented in Sec. IV. Note particularly that $K_{ll'}(r)$ is tridiagonal, like $L_{ll'}^{(ba)}$, in this approximation. It may thus prove more practical to obtain $K_{ll'}(r)$ first, and then to diagonalize it, than to follow the procedure of Sec. III B in the weak-field range.

Let us then examine how $L_{ll'}^{(ba)}$ varies with increasing r. The diagonal element $L_{ll}^{(ba)}$ is proportional to $\sin^2\phi_l(r)=[1-\cos 2\phi_l(r)]/2$; the $\frac{1}{2}$ factor of this expression is constant, but the rapid oscillations of $\cos 2\phi_l/2$ cancel the integrated contribution of any additional constant (or slower varying) factor. [The occurrence of a factor oscillating with the double frequency $2\phi_l(r)$ is a feature of the phase-amplitude procedure of Sec. III A.] The factor $\sin^2\phi_l(r)$ also occurs in the expression of the off-diagonal elements of $L_{ll'}^{(ba)}$ when cast in the form

$$\begin{aligned} L_{ll-2}^{(ba)} &= -\pi\beta r^2 U_{ll-2}\alpha_l(r)\alpha_{l-2}(r)\sin\phi_l(r)\sin\phi_{l-2}(r) \\ &= -\pi\beta r^2 U_{ll-2}\alpha_l\alpha_{1-2}[\cos(\phi_l-\phi_{l-2}) \\ &\qquad +\sin(\phi_l-\phi_{l-2})\cot 2\phi_l] \\ &\quad \times\sin^2\phi_l \ . \end{aligned} \tag{32}$$

In this expression the factor $\cot 2\phi_l$ also oscillates rapidly but its poles do not contribute to the relevant integration by principal part. The key term in the brackets is thus $\cos(\phi_l-\phi_{l-2})$, whose argument decreases smoothly from 2π to 0 as r increases. The variation of this term—positive at low r, then dropping rapidly to negative values over an extended range, and finally positive again (Fig. 4)—has a decisive influence on the structure of the whole matrix $K_{ll'}(r)$ at any fixed value of r.

Figure 5 shows the trend of diagonal and off-diagonal elements of $K_{ll'}(r)$ as functions of both l and r. The values of these elements are scaled by the numerical factor $\beta r^{7/2}$ so as to remain comparable throughout the range $0<r\leq 200$ a.u. The sign of the diagonal elements is negative because the diamagnetic potential is positive. Their magnitude tends to increase with l, then decreasing abruptly at the largest l values, where the centrifugal barrier excludes electrons from the diamagnetic action.

The sign of the off-diagonal elements $K_{ll-2}(r)$ alternates as a function of l, in contrast to the sign of diagonal elements, reflecting the oscillation of the cosine factor in Fig. 4. The whole matrix would thus resolve into three independent submatrices if one off-diagonal element were to vanish at each node of K_{ll-2} separating the ranges of its positive and negative values. These nodes do not actually often coincide with even values of l. Sufficiently small values of K_{ll-2} do, however, occur very often in the proximity of the first node in l, thus effectively separating a low-l submatrix. The corresponding effect is more elusive for the second node. Both nodes will nevertheless prove helpful in interpreting the eigenvalues and eigenvectors of $K_{ll'}(r)$ to be presented in Sec. IV.

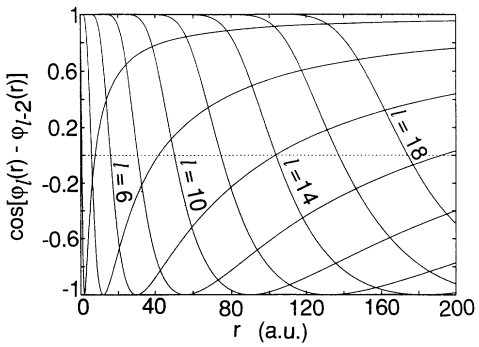

FIG. 4. Dependence on r of the $\cos[\phi_l(r)-\phi_{l-2}(r)]$ of Milne phase differences.

The alternation of sign of the off-diagonal K_{ll-2}, as l increases, combined with the uniform sign of the diagonal K_{ll}, implies that the ratio K_{ll-2}/K_{ll} alternates in sign. This ratio is indeed negative at low- and high-l values and positive at intermediate l, where the $\cos(\phi_l-\phi_{l-2})$ is also negative. We recall here that a sign reversal of the ratio of off-diagonal and diagonal elements had a central role in the study of localization of Ref. [13], where the reversal was dubbed a "conjugation." No immediate connection between these sign reversals is apparent at this point.

IV. THE EIGENPHASE SHIFTS AND EIGENVECTORS AT SHORT RANGES

The theoretical framework laid out in Sec. II provides a new perspective on the evolution of atomic and molecular nonseparable wave functions. In this study of Rydberg diamagnetism we examine the eigenphase shifts and eigenvectors of the short-range reaction matrix $K_{ll'}(r)$, as functions of the radial distance r, evaluated in accordance with Sec. III. We do so by exploring only the weak-field range $r<200$ a.u., sufficient to reach the effective onset of the approximate separability, which was outlined in Sec. II C and requires further analytic development.

The eigenshifts $\delta_p(r)$ and the eigenvectors $\langle l|p(r)\rangle$ have been calculated through the interplay of the diagonal and off-diagonal parts of the matrix equation (21). The kernel $M_{ll'}^{(pp')}$ of this equation simplifies in the weak-field range through disregard of the very small phase shifts $\delta_p(r)$ and $\delta_{p'}(r)$ in Eq. (21'); thereby the indices (p,p') also drop out replacing Eq. (21') by

$$M_{ll'}=-\pi\beta r^2\alpha_l(r)\sin\phi_l(r)U_{ll'}(r)\sin\phi_{l'}(r)\alpha_{l'}(r) \ . \tag{33}$$

The factor $\sin(\delta_p-\delta_{p'})$ in the denominator of (23) reduces similarly to $\delta_p(r)-\delta_{p'}(r)$, which is on the order of $\beta r^{7/2}$.

A. Eigenphase shifts

The complete set of calculated eigenphase shifts is presented in Fig. 6(c), for a field strength $B=5$ T, $r\leq 200$ a.u., and $E=0$ in Eq. (9). In this range the ratio of the diamagnetic and Coulomb potentials remains $\leq 10^{-4}$, and only ten phase shifts become appreciable on the vertical scale of Fig. 6(c). Figure 6(a) shows the first four non-negligible eigenphase shifts emerging from the centrifugal barrier on an enlarged scale, $r\leq 25$; Fig. 6(b) shows the first seven shifts for $r\leq 70$ a.u.

These figures display a complicated network of avoided crossings; all the intersections are actually avoided as no crossing is compatible with the pole singularity of Eq. (23). This large, seemingly surprising, amount of channel interaction stems from the commutability of diamagnetic

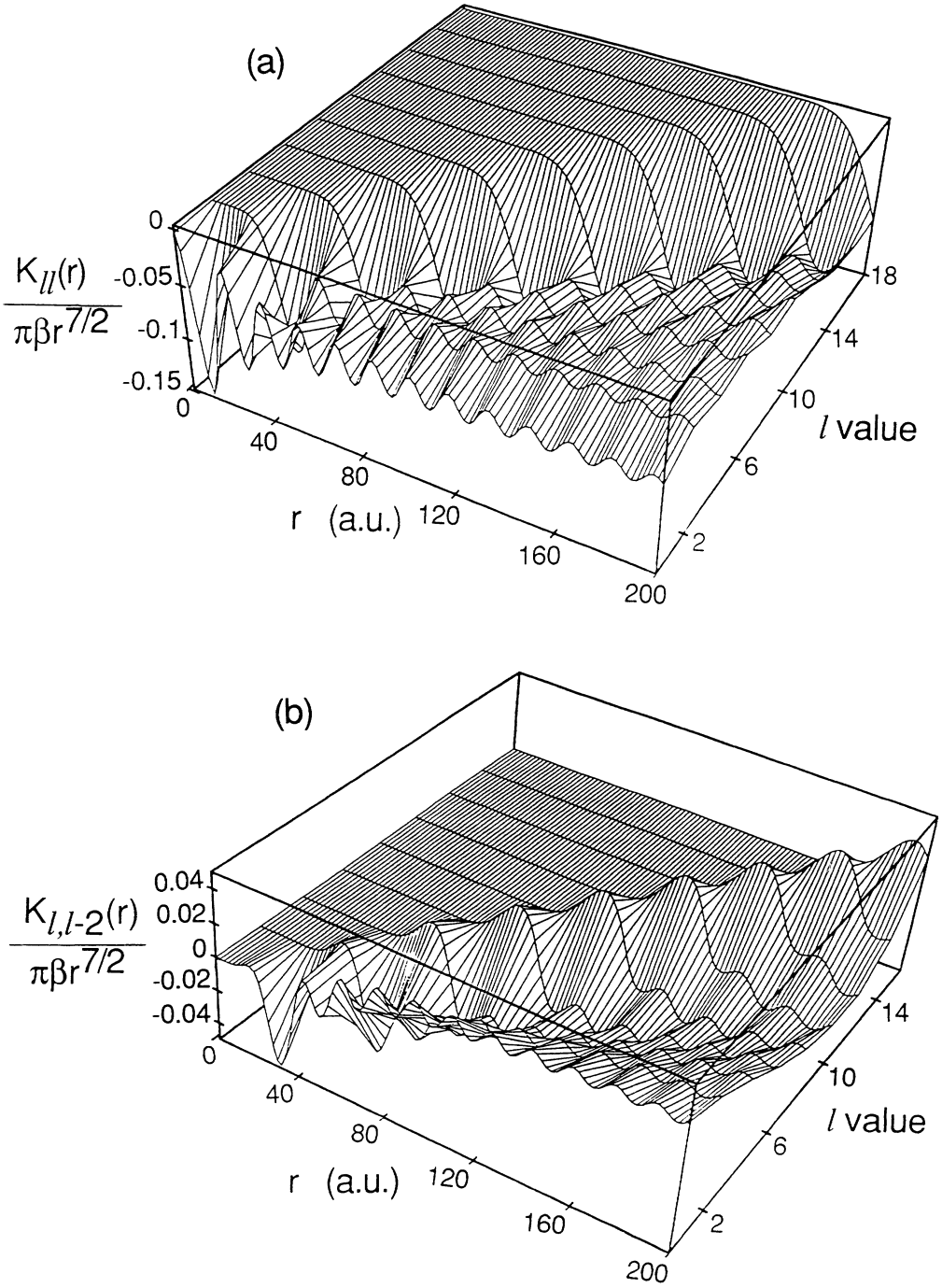

FIG. 5. Dependence on (r,l) of (short-range) reaction matrix elements: (a) $K_{ll}(r)$ and (b) $K_{l\,l-2}(r)$, in units of $\pi\beta r^{7/2}$.

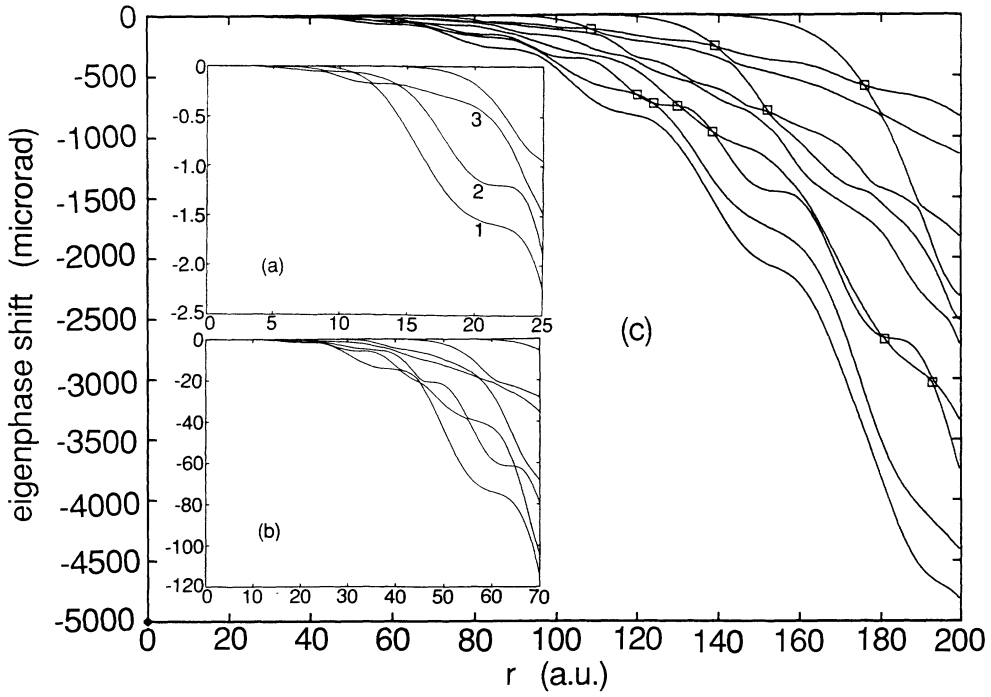

FIG. 6. Eigenphase shifts $\delta_p(r)$ of the (short-range) reaction matrix $K_{ll'}(r)$ for three ranges of r: (a) $r \leq 25$ a.u., (b) $r \leq 70$ a.u., (c) $r \leq 200$ a.u. □, avoided crossings treated as diabatic.

and Coulomb potentials noted in Sec. II B. Varying the field strength up to 10 T would merely stretch the ordinates of Fig. 6, without distorting its curves, because the matrix (33) is linear in β. [The eigenvectors $\langle l|p(r)\rangle$ are similarly independent of β in our range.]

Even though all channel crossings are avoided in principle, it is a good approximation to treat many of them [ten of them in Fig. 6(c)] as *diabatic*. This classification implies that each of the pair of channel labels, and the corresponding eigenvector of $K_{ll'}(r)$, remains practically unaffected by disregarding the occurrence of the crossing. This is the case specifically if the eigenvectors of the two channels lie in different subspaces of the l parameters.

B. Anatomy of channel mixing at very short ranges

Consider here the crossing in Fig. 6(a) at $r=14.3$ a.u. and $\delta \sim 2\times 10^{-7}$, which seems, but is not, diabatic. At this range only three channels have non-negligible phase shifts. The channel labeled "1" remains unaffected by the crossing of "2" and "3." All three of these eigenvectors can be identified, as r traverses the crossing, by the variations of their spherical coordinates (θ,φ) with respect to Cartesian axes $l=\{0,2,4\}$, with $l=4$ corresponding to $\theta=0$ and with $l=0$ in the $\varphi=0$ plane. Figure 7(a) shows the variations of (θ_1,φ_1), (θ_2,φ_2), and (θ_3,φ_3); Fig. 7(b) the angle Θ between the directions of (θ_2,φ_2) at r and its direction at the *initial* radius $r=13.5$. The final value of Θ falls well short of 90°. If Θ had reached 90°, the crossing could have been viewed as diabatic, by interchanging the labels of "2" and "3" and keeping each vector in a fixed direction.

In this example, the vector 1 maintains its direction, orthogonal to the plane of 2 and 3. In general, one might expect the plane of two vectors involved in the crossing to tilt in the multidimensional space of parameters l.

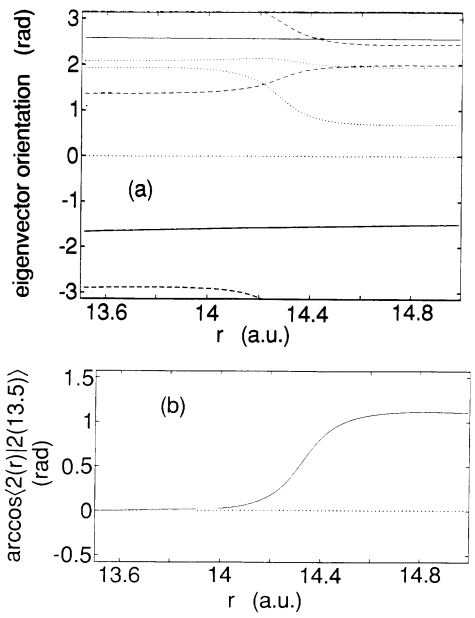

FIG. 7. Orientation of the eigenvectors $p\equiv\{1,2,3\}$ as r increases through the avoided crossing at $r\sim 14.5$ a.u. (a) Spherical coordinates, solid line: (θ_1,φ_1); long dashes: (θ_2,φ_2); short dashes: (θ_3,φ_3) in the basis space $l\equiv\{0,2,4\}$. (b) Angle $\Theta=\arccos\langle 2(r)|2(13.5)\rangle$.

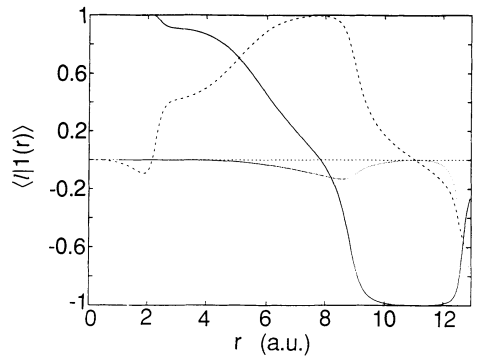

FIG. 8. Components $\langle l|1(r)\rangle$ of the eigenvector with the largest phase shift $\delta_1(r)$ in the range $0<r\leq 13$ a.u.: solid line: $l=0$; dashed line: $l=2$; dotted line: $l=4$.

However, the tilt appears to be negligible for most of the numerous crossing displayed in Fig. 6.

Figure 6(a) also shows three avoided crossings at $r<14$ involving all the three eigenvectors labeled above as $\{1,2,3\}$ whose components are restricted in this range to $l=\{0,2,4\}$. Figure 8 plots the values of the three components $\{\langle 0|1(r)\rangle,\langle 2|1(r)\rangle,\langle 4|1(r)\rangle\}$ through the range $0\leq r\leq 13$ a.u. The curve $\langle 2|1(r)\rangle$ displays a feature of *general significance,* namely, negative values over a very brief range near $r=0$, corresponding—through orthogonality—to initially positive values of the component $\langle 0|2(r)\rangle$. These signs are *promptly reversed* as r increases, owing to the rapid drop and sign reversal of $\cos(\phi_2-\phi_0)$ displayed in Fig. 4. The similar behavior of the $\cos(\phi_l-\phi_{l-2})$ for all l values, as soon as $\phi_l(r)$ departs from $l\pi$, implies full generality of such prompt sign reversals.

Three avoided crossings among the eigenvectors $\{1,2,3\}$ are also apparent in the range of Fig. 6 covered by the plots of $\langle l|1(r)\rangle$ in Fig. 8. The crossing of $|1\rangle$ and $|2\rangle$ at $r\sim 9$ a.u. generates in Fig. 8 a sudden drop of $\langle 0|1(r)\rangle$ from ~ 0 to -1, accompanied by a drop of $\langle 2|1(r)\rangle$ from 1 to ~ 0. [The earlier drop of $\langle 0|1(r)\rangle$ from ~ 1 to ~ 0 near $r=5$ a.u., accompanied by the rise of $\langle 2|1(r)\rangle$ from 0 to 1, reflects instead no evidence of another crossing.] The second crossing in Fig. 6(a) at $r\sim 11$ a.u. involves the eigenvectors $|2(r)\rangle$ and $|3(r)\rangle$ exerting no obvious influence on the components $\langle l|1(r)\rangle$ plotted in Fig. 8. The third crossing, at $r\sim 12.5$ a.u., involves $|1(r)\rangle$ and $|2(r)\rangle$ once again, manifesting itself in Fig. 8 through sharp variations of all the components $\langle l|1(r)\rangle$.

A final comment concerns the (adiabatic looking) closeness of approach at two avoided crossings shown in Fig. 6(a) at $r\sim 11$ and $r\sim 14.5$ a.u. This effect has been traced to destructive interferences among the terms of the $\sum_{ll'}$ in the square brackets of Eq. (23).

C. Eigenvectors

Figure 9 shows histograms of all the eigenvector components $\langle l|p(r)\rangle$ with non-negligible δ_p at $r=170$ a.u. a value selected to illustrate most clearly the subdivision into three blocks anticipated in Sec. III D. The values of the index $p\equiv\{1,2,\ldots 10\}$ are labeled in the order of descending values of $|\delta_p(170)|$.

The low-l block consists of $p\equiv\{3,7,9\}$. The eigenvector $p=3$, corresponding to the largest of the three eigenvalues displays the alternation of sign of the three "large" components with $l=\{0,2,4\}$. The remaining components are small. This eigenvector thus matches the characteristics of a state localized at a high potential, as anticipated from Ref. [13] at the outset of Sec. II. Similarly the eigenvector $\langle l|9\rangle$ has its largest components at $l=0,2,4$ with uniform sign, corresponding to a localization at low potential. The localization of the eigenvector $\langle l|7\rangle$ in physical space is less clear from Fig. 9. [The lack of detailed correspondence between the eigenvectors of $K_{ll'}(r)$ evaluated at a fixed r and those studied in Ref. [13] has been anticipated and explained in Sec. II C.]

The block of eigenvectors centered at intermediate-l values consists of $p=\{2,4,5,6,8\}$ whose increasing number of nodes corresponds to a decrease in $|\delta_p|$ values. This contrast reflects the negative value of the $\cos(\phi_l-\phi_{l-2})$ characteristic of this block, anticipated in Sec. III D.

The third, high-l, block consists of the two eigenvectors $\langle l|1\rangle$ and $\langle l|10\rangle$ with highest and lowest $|\delta_p|$, respectively. The low value of $|\delta_{10}|$ reflects the early stage of development of its eigenvector, just emerging from the centrifugal barrier. The high value of $|\delta_1|$ reflects the next stage of development of the eigenvector, whose wave function $\sim\alpha_l(r)\sin\phi_l(r)$ with $l=16$ has the largest amplitude α_l and the longest wavelength over the range of r preceding $r=170$ a.u. [Both of these characteristics hinge on the low value of $d\phi_l/dr$ at $r\sim 170$ a.u., representing the low electron velocity near the exit from the barrier and the lower value of the acceleration that persists through a range of $r\sim l(l+1)$.] These features of the eigenvector $|1(r)\rangle$ at $r\simeq 170$ a.u. will be illustrated further in Sec. IV E.

The subdivision in blocks, primarily between the second and third ones, is vitiated as r varies by the mixing of eigenvectors at channel crossings as well as by non-negligible values of off-diagonal elements $K_{ll'}(r)$. For example, the crossing at $r\sim 190$ a.u. and $|\delta_p|\sim 0.0016$ between the eigenvectors with $p=7$ and 10 (labels assigned at $r=170$ a.u.) intermixes even eigenvectors of the first and third blocks, at least locally. The eigenvector $p=1$, sharply localized at $l=9$ when $r=170$ a.u., spreads over several values at $r\sim 195$ a.u., because the matrix element $K_{16,14}$ is not negligible in the intervening range.

D. Radial development of the low-l block

The three eigenvalues of the low-l block of $K_{ll'}(r)$, labeled as $\{\delta_3(r),\delta_7(r),\delta_9(r)\}$ at $r=170$ a.u., experience diabatic crossings throughout the range $100<r<200$ a.u. with minor exceptions in the case of $\delta_7(r)$. Their variations through this range appear accordingly rather free from influences of interactions with other eigenchannels. Figure 10 displays the growth of these three eigenphase shifts, lifted out of Fig. 6(c).

The rate of growth of each curve is clearly oscillatory,

thus suggesting at first blush a residual influence of avoided crossings. These oscillations do instead reflect simply those of the factor $\sin^2\phi_l$ of Eq. (32), which are transmitted to $\delta_p(r)$ through the $\int_0^r dr' L_{ll'}^{(ba)}(r')$. This is verified by plotting the nodes of the second derivative, $d^2\delta_p/dr^2$, and comparing them with the periodicity of $\sin^2\phi_l$. Recall that $\phi_l(r)$ itself grows as $\sqrt{8r}$ to $O(l(l+1)/r)$ and thus independently of l [26]. Accordingly both the nodes of $d^2\delta_p/dr^2$ and the Milne phases $\{\phi_0,\phi_2,\phi_4\}$ were plotted against $\sqrt{r}$, the slope of the nodes being found linear and twice as large as those of the $\{\phi_l(r)\}$.

E. Sequential leapfrogging into the middle-l block, through quasidiabatic crossings

Most of the avoided crossings observed in Fig. 6(c), other than previously discussed, fall into a single class

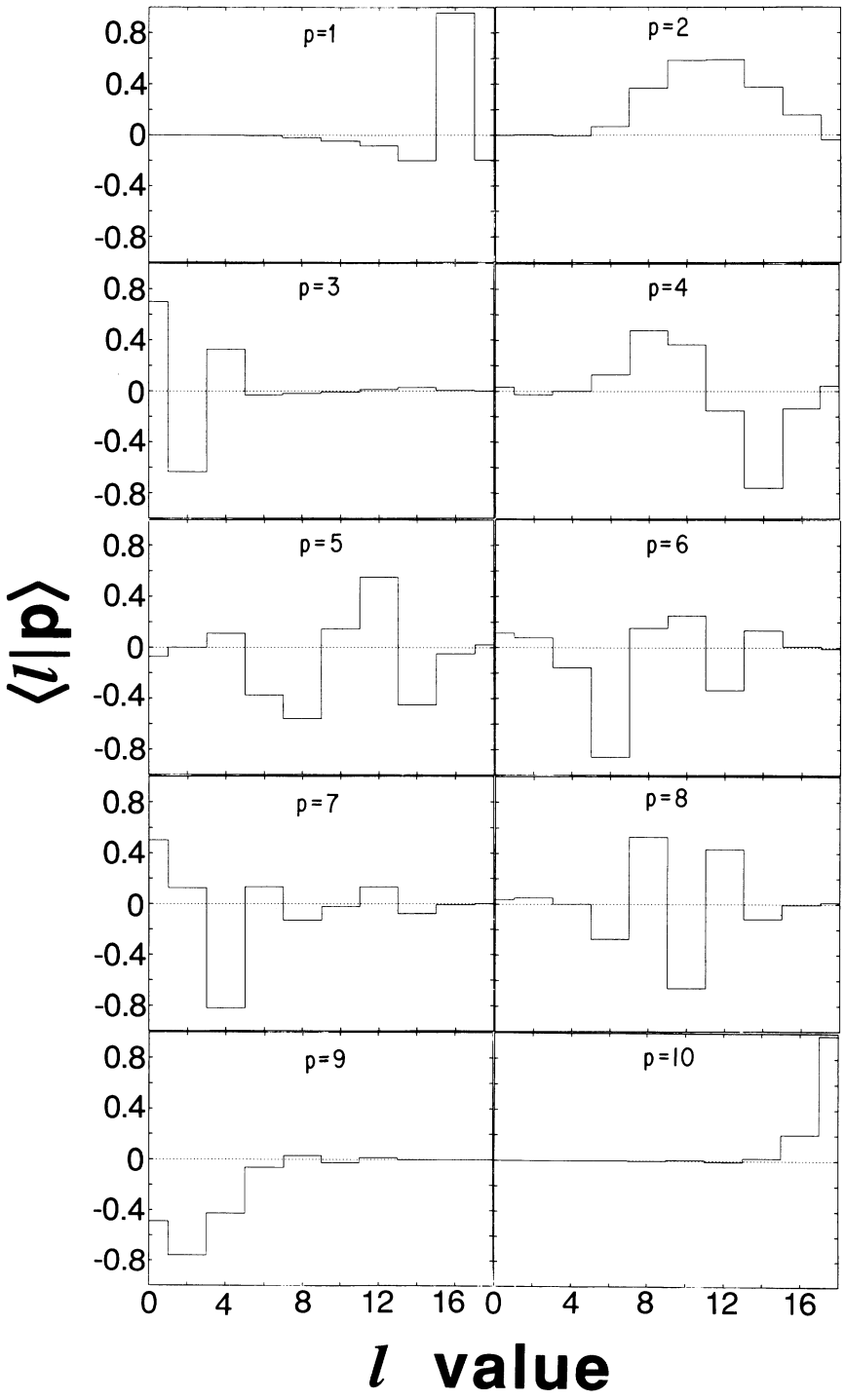

FIG. 9. Histograms $\langle l|p\rangle$ of the eigenvector components at $r=170$ a.u., with p values in order of decreasing $|\delta_p(170)|$.

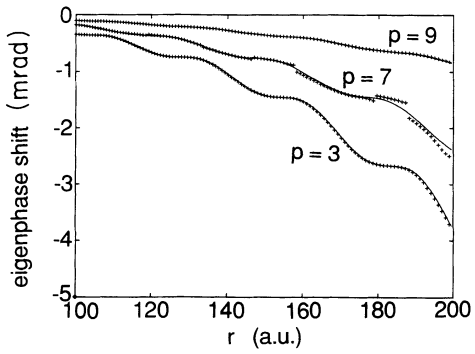

FIG. 10. Eigenphase shifts of the low-l block, labeled by $p=\{3,7,9\}$ in descending order of $|\delta_p(170)|$. Solid line: $\delta_p(r)$ eigenvalues of $K_{ll'}$ with $(l,l')\equiv\{0,2,4\};+$, $\delta_p(r)$ of full matrix $K_{ll'}(r)$.

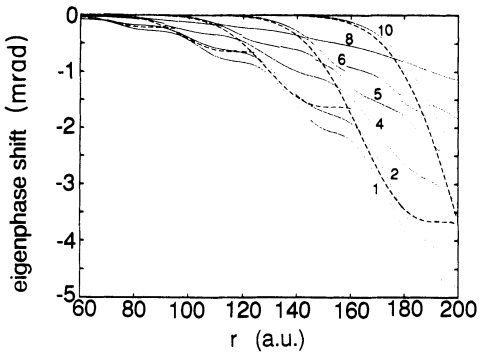

FIG. 11. Dotted line: Eigenvalues $\delta_p(r)$ with $p=\{1,2,4,5,6,8,10\}$ in descending order of $|\delta_p(170)|$. Breaks in some curves reflect removal from Fig. 6(c) of points indicated by + in Fig. 10. Dashed line: $\arctan\int_0^r dr' M_{ll}(r')$ for $l=\{10,12,14,16,18\}$.

emphasized in the Fig. 11 graphs. This class may be characterized with reference to the remark in Sec. IV C that the largest component of the eigenvector with highest $|\delta(r)|$ value at $r=170$, labeled there as $|\delta_1|$, has the near-maximal l value, namely, $l=16$. Tracing back this eigenvector in Fig. 11 [or 6(c)] on a *diabatic* path, we notice that it first emerges from the centrifugal barrier at $r\sim 120$ a.u. and that it experiences as many as *five* avoided crossings within the range $120<r<170$ a.u. Many of these crossings appear to be quite adiabatic, rather than quasidiabatic; the component $\langle 16|1(r)\rangle$ has nevertheless maintained its initial predominance. [The appreciable $\langle 18|1(r)\rangle$ component at $r=16$ appears to have been generated by the coupling within the high-l block.]

Inspection of the five quasidiabatic tracks indicated on Fig. 11 by dashed lines, and of the relevant eigenvector components, shows the persistent dominance of their initial l component to be strikingly general. These lines represent the dominant contribution to each $\delta_p(r)$ by a single diagonal component $M_{ll}(r)$, Eq. (33), i.e., $\arctan\int_0^r dr' M_{ll}(r')$. This dominance subsides, merging into the set of middle-l block eigenvectors, only after the high-l eigenvector has been leapfrogged by that with the next higher l.

Inspection of the various plots of $\delta_p(r)$ versus r, and reference to the histograms of eigenvector components in Fig. 9 and in our files, suggests that we have in fact exhausted the diversity of crossing phenomena in the range $r<200$ a.u.

V. DISCUSSION

The motion of a Rydberg electron, subject to centrifugal, Coulomb, and magnetic forces is nonseparable owing (in part) to noncommutativity of the operators that represent centrifugal and magnetic forces. The theoretical framework described in Sec. II localizes the critical range of noncommutative interactions at intermediate radial distances. The electron's response to the combined actions in this range can be evaluated by a rather transparent phase-amplitude procedure described analytically in Sec. III. Section IV contains the application of this procedure and an interpretation of several of its results.

Remarkably, the construction of eigenfunctions $F_{ll_0}(r)$ by this method is rather trivial in the range of weak diamagnetism, but sheds little light on the dynamical process. It is the study of eigenvalues and eigenvectors of the short-range reaction matrix that proves rewarding.

Completion and implementation of the program outlined in Sec. II requires the development of quasiseparable wave functions at larger radial distances where the centrifugal field no longer dominates but remains non-negligible. It also requires developing a subsidiary procedure to match the quasiseparable wave functions to those constructed in the intermediate range. Achievement of these goals should afford confining the phase-amplitude procedure to a rather narrow strip of the (r,l) domain. Work in this direction is currently underway, and will be reported later.

The broad relevance of the present development to multiparticle systems has been noted in Sec. I and through occasional further remarks. It has also been presented more extensively in a conference paper [27].

Our initial exploration of wave functions in the critical intermediate range, previously treated by opaque variational (or equivalent) procedures, might give impetus to analogous studies of other atomic and molecular problems. This hope has encouraged publication of a progress report at this time.

Note added in proof. Numerical experience with integration of (14), extended to $r\sim 1600$ a.u., has shown it preferable to the more articulate procedure developed in the following Sec. III B. That is, integration of (14) may be followed by determining $\langle l|p(r)\rangle$ and $\delta_p(r)$ directly from (16) and (20).

ACKNOWLEDGMENTS

This work has been supported by NSF Grants No. PHY 89-18304 and No. 90-19966. We are indebted to F. Robicheaux for the construction of Fig. 2 and to him and to John Bohn for multiple discussions and critical advice.

[1] A. R. P. Rau, Phys. Rev. A **16**, 613 (1977).
[2] F. A. Jenkins and E. Segrè, Phys. Rev. **55**, 52 (1939); L. I. Schiff and H. Snyder, *ibid.* **55**, 59 (1939).
[3] W. R. S. Garton and F. S. Tomkins, Astrophys. J. **158**, 839 (1969); K. T. Lu, F. S. Tomkins, and W. R. S. Garton, Proc. R. Soc. London, Ser. A **362**, 421 (1978), and references therein.
[4] D. Delande *et al.*, Phys. Rev. Lett. **66**, 141 (1991); C. H. Iu *et al.*, *ibid.* **66**, 145 (1991).
[5] A. Holle *et al.*, Phys. Rev. Lett. **56**, 2594; **57**, 2789 (1986).
[6] D. Wintgen and H. Friedrich, Phys. Rev. Lett. **57**, 571 (1986); D. D. Delande and J. C. Gay, *ibid.* **57**, 2006 (1986).
[7] C. J. Goebel (unpublished, 1980).
[8] See, e.g., M. J. Seaton, Rep. Prog. Phys. **46**, 167 (1983).
[9] U. Fano, Phys. Rev. A **37**, 4037 (1988); Comments At. Mol. Phys. **19**, 253 (1988).
[10] Qiaoling Wang and C. H. Greene, Phys. Rev. A **44**, 1874 (1991); P. F. O'Mahony and F. Mota-Furtado, Phys. Rev. Lett. **67**, 2283 (1991); S. Watanabe and H. Komine, *ibid.* **67**, 3327 (1991); Qiaoling Wang and C. H. Greene, Phys. Rev. A **44**, 7448 (1991).
[11] See, e.g., U. Fano. J. Opt. Soc. Am. **65**, 975 (1975)
[12] U. Fano, Phys. Rev. A **26**, 2401 (1981); also U. Fano and A. R. P. Rau, *Atomic Collisions and Spectra* (Academic, New York, 1986), Chaps. 10 and 11.
[13] U. Fano, F. Robicheaux, and A. R. P. Rau, Phys. Rev. A **37**, 3655 (1988).
[14] See, e.g., the joint discussion of these examples in U. Fano, Phys. Rev. A **24**, 2660 (1980).
[15] See, e.g., A. F. Starace and G. L. Webster, Phys. Rev. A **19**, 1629 (1979); C. H. Greene, *ibid.* **23**, 661 (1981).
[16] See, e.g., Ref. [12]; S. Watanabe and H. Komine, Ref. [10].
[17] W. E. Milne, Phys. Rev. **35**, 863 (1930); F. Robicheaux *et al.*, Phys. Rev. A **35**, 3619 (1987).
[18] (a) C. Zemach, Nuovo Cimento **33**, 939 (1964); (b) A. Degasperis, *ibid.* **34**, 1667 (1964); (c) F. Calogero, *Variable Phase Approach to Potential Scattering* (Academic, New York, 1967), Chap. 19.
[19] U. Fano and A. R. P. Rau, *Atomic Collisions and Spectra* (Academic, Orlando, 1986), Chap. 8.
[20] R. G. Newton, *Scattering Theory of Waves and Particles* (McGraw-Hill, New York, 1966).
[21] U. Fano, in *Fundamental Processes of Atomic Dynamics,* edited by J. Briggs *et al.* (Plenum, New York, 1988), pp. 41–49.
[22] See, e.g., Fig. 5 of H. A. Bethe and E. Salpeter, *Quantum Mechanics of One and Two Electron Systems* (Springer, Berlin, 1957).
[23] E. Sidky and F. Robicheaux (unpublished).
[24] R. Bellman and R. Kalaba, J. Math. Mech. **8**, 683 (1959); R. Bellman and G. M. Wing, *An Introduction to Invariant Imbedding* (Wiley-Interscience, New York, 1975).
[25] See, e.g., U. Fano, and A. R. P. Rau, Ref. [19], pp. 44–45 and 116 and 117.
[26] See, e.g., *Handbook of Mathematical Functions,* edited by M. Abramowitz and I. B. Stegun (Dover, New York, 1965), p. 365. The eigenfunction of H_{0l}, Eq. (2), for $E=0$ is known to be represented through the Bessel function $J_{2l+1}(\sqrt{8r}\,)$; the extension of this expression to $E\neq 0$ by R. E. Langer appears in Phys. Rev. **51**, 675 (1937).
[27] U. Fano, in *Dynamical Scaling in Chemical Physics,* edited by J. Avery *et al.* (Kluwer, Amsterdam, 1992).